The calculation of some Batchelor flows: The Sadovskii vortex and rotational corner flow

D. W. Moore,[a] P. G. Saffman, and S. Tanveer[b]
Applied Mathematics, California Institute of Technology, Pasadena, California 91125

(Received 27 August 1987; accepted 29 January 1988)

Steady, inviscid, incompressible, two-dimensional flows with vortex patches bounded by vortex sheets (Batchelor flows) are calculated numerically. Two particular cases are considered: the vortex on a plane wall (Sadovskii vortex) and the vortex in a right-angled corner. Nonlinear integral equations are derived for the shape of the bounding vortex sheet which are solved numerically. Two different formulations are employed to check the results. Previous results by Sadovskii [Appl. Math. Mech. **35**, 773 (1971)] and Chernyshenko (Royal Aircraft Establishment library translations Report No. 2133, 1983) for specific values of the parameters are confirmed. Only symmetrical solutions are found to exist.

I. INTRODUCTION

The importance of inviscid flows in which patches of uniform vorticity are separated from each other and from an external irrotational flow by vortex sheets arises from the fact that they are plausible limits of viscous flows at infinite Reynolds number. Thus, as pointed out by Batchelor,[1] flows of this type could describe the wake behind a body at infinite Reynolds number, or flow down a step. A typical "Batchelor flow" is sketched in Fig. 1.

When Batchelor made this proposal, it was not possible to compute flows of this type and so the first attempt at a detailed calculation made the additional assumption of slenderness.[2] However, the assumption of slenderness does not yield a linear problem. This is because the boundary velocity is proportional to the thickness and so the boundary pressure in a slender rotational eddy is a constant plus a term proportional to the square of its thickness. Thus pressure matching across the boundary of the eddy leads to a nonlinear integral equation for its shape, which Childress solved numerically by fixed-point iteration. Existence of solutions of the nonlinear integral equation was proved rigorously. Childress studied several flows of this type, but the one of most interest to us is sketched in Fig. 2(a). He found a one-parameter family of such solutions and for each nondimensional amplitude y_m/L there was a unique vorticity ω given by

$$\omega L/U = 5.05(L/y_m)^{1/2}. \tag{1}$$

Sadovskii[3] calculated four members of the family without assuming slenderness. He obtained a coupled pair of nonlinear integral equations for the profile and vortex-sheet strength. No details of the numerical method were given but one can infer, from the form in which the integral equations are written, that fixed-point iteration was used. Sadovskii noticed that the family is terminated by a solution in which the vortex sheet is absent; this is the same solution subsequently calculated by Pierrehumbert[4] and—with an error corrected—by Saffman and Tanveer.[5]

More recently Smith[6] repeated Childress's work and extended[7] the calculations of Sadovskii[3] to find profiles over the whole range of the controlling parameter. In the latter work, a hybrid method was used in which finite differences were employed in the interior and an integral representation in the exterior. Fixed-point iteration was used to solve the resulting system.

There has been less work on rotational corner flows, sketched in Fig. 2(b), but Chernyshenko[8] gave one member of the family. He used a finite difference method in which a pseudotime was introduced.

Our interest was aroused both by numerical discrepancies between Smith's[7] and Sadovskii's[3] results and by Smith's[7] suggestion that there might be Sadovskii vortex solutions that lack the fore and aft symmetry characterizing previous work.

In Sec. II we consider some general features of Batchelor flows, with particular emphasis on the degrees of freedom of such solutions. We also consider the nature of the flow at the cuspidal separation and reattachment points, with a view to incorporating the correct behavior into our solutions.

In Sec. III we describe two methods of solution, giving

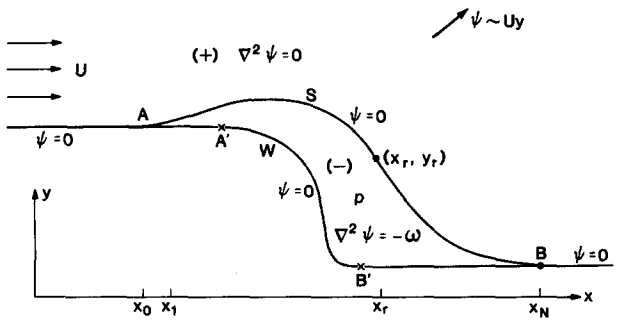

FIG. 1. A typical Batchelor flow. The semi-infinite parallel planes $-\infty AA'$ and $B'B\infty$ are joined by a smooth step to form the boundary W. A vortex sheet S separates an irrotational " + " region from a region " − " or P of uniform vorticity ω. Axes are chosen with OX parallel to $-\infty AA'$ and $B'B\infty$ and (x_r, y_r) $(r = 0,1,...,N)$ provide a discrete description of S.

[a] Permanent address: Department of Mathematics, Imperial College, London, England.

[b] Permanent address: Department of Mathematics, Virginia Polytechnic Institute and State University, Blacksburg, Virginia 24061.

 0031-9171/88/050978-13$01.90

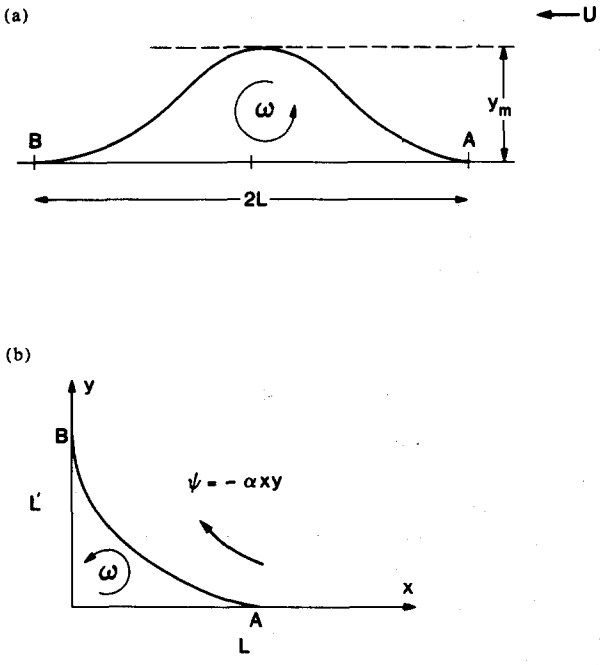

FIG. 2. Sketches of the Sadovskii vortex (a) and the rotational corner flow (b). (It is convenient to reverse the flow direction with respect to Fig. 1, to make $\omega > 0$.)

full details only for the Sadovskii vortex case. Both methods use a Fourier representation of the shape [Eq. (18)] which has the correct cuspidal behavior built in. Method 1 is basically a vortex representation of the velocity field, the vortex sheet, and the vortex patch yielding boundary integrals over the interface between rotational and irrotational flow. The contributions from the patch are reduced to boundary integrals by using the methods of contour dynamics. Method 2 is based on a boundary-integral representation of the harmonic part of the streamfunction.

Both methods use Newton iteration to solve the discretized equations so that we can look for bifurcations to solutions that lack fore and aft symmetry. The principal technical problem to be faced in either method is the accurate evaluation of the contributions to the various integrals from the cuspidal neighborhoods of the separation and reattachment points, where the integrands become large and rapidly varying. We attacked this difficulty by introducing suitable canceling functions, described in Sec. III C, and comparison with the exact solution for a stagnant corner suggests that we have achieved adequate resolution.

Section IV describes our results for the Sadovskii vortex. We have tried to establish numerical convergence and in Sec. IV A we give details of one particular case as the numerical parameters are changed. In Sec. IV B we compute a family of Sadovskii vortices and compare with previous results. We differ slightly with Smith[7] while agreeing with Sadovskii,[3] except for the limiting case of no vortex sheet. We examine the Jacobian of the discretized equations and find no evidence for bifurcations into nonsymmetrical solutions.

Section V gives results for the corner. Again there appear to be no bifurcations. We experienced convergence difficulties in this case, particularly in the weak vortex-sheet limit.

Finally in Sec. VI we summarize our findings. Interest in the Sadovskii vortex has been increased since Fornberg[9] suggested, on the basis of numerical solution of the Navier–Stokes equations at high Reynolds numbers, that the Sadovskii vortex (plus its image) could represent the wake. We make a quantitative comparison in Sec. VI.

II. PROPERTIES OF BATCHELOR FLOWS

A. Degrees of freedom

We shall define a Batchelor flow to be a steady solution of the Euler equations for a homogeneous incompressible fluid in which regions of constant or zero vorticity are separated by vortex sheets and which contains a vortex sheet that is also a dividing streamline. Such a flow is sketched in Fig. 1. Fluid flows with velocity U over a step in the boundary W and a streamline S separates at A and reattaches at B. It is clear that if S is prescribed, the boundary-value problem for ψ sketched in Fig. 1 has a unique solution. If the configuration is to be steady then the pressure must be continuous across S. Bernoulli's theorem shows that on S

$$\begin{aligned} p_+ + \tfrac{1}{2}\rho(\nabla\psi_+)^2 &= h_+ \quad \text{on } S_+, \\ p_- + \tfrac{1}{2}\rho(\nabla\psi_-)^2 &= h_- \quad \text{on } S_-, \end{aligned} \tag{2}$$

so that continuity of pressure requires

$$(\nabla\psi_+)^2 - (\nabla\psi_-)^2 = q^2, \tag{3}$$

where

$$q^2 = 2(h_+ - h_-)/\rho. \tag{4}$$

In these equations, ρ is the uniform density, p is pressure, and h_+ and h_- are the total heads on either side of S.

We denote the fluid velocities on either side of S by q_+ and q_-. Then (3) gives

$$\gamma(q_+ + q_-) = -q^2, \tag{5}$$

where

$$\gamma = q_- - q_+, \tag{6}$$

which shows that, unless $q = 0$, S must be a vortex sheet of strength γ.

Furthermore, if $q \neq 0$, q_+ and q_- cannot both vanish at A or at B and the only possibility is that $q_- = 0$ and $q_+ = q$, corresponding to tangential separation and reattachment. Then we have

$$\gamma(A) = \gamma(B) = -q, \tag{7}$$

as remarked by Sadovskii.[3] We will employ (7) as a check on the accuracy of the vortex-sheet method of Sec. III A.

If $q = 0$, however, it was shown by Saffman and Tanveer[5] that S must depart from A at an angle $\pi/2$ to the wall W. This change in the geometry renders $q \to 0$ a singular limit, as pointed out by Smith.[6]

We wish to show that, given U, the vorticity ω, and the location of the separation point A, then q, S, and the reattachment point B are determined. We have no rigorous uniqueness theorem and we fall back on a counting argument for the discretized equations. We describe S by coordinates (x_r, y_r), where $r = 0,1,2,\ldots,N$. Since A is known, (x_0, y_0) is known, and since the height of the step is known,

y_N is known. Thus the unknowns are $y_1 y_2,...,y_{N-1}$, x_N, and q, a total of $N+1$. Now the boundary-value problem for the streamfunction ψ uniquely determines q_+ and q_- at (x_r,y_r), so that the application of the pressure condition (3) at (x_r,y_r) $(r=0,1,...,N)$ leads to $N+1$ equations,

$$R_r \equiv q_+^2(r) - q_-^2(r) - q^2 = 0 \quad (r=0,1,...,N), \tag{8}$$

where

$$q_\pm(r) = q_\pm(x_r,y_r) \quad (r=0,1,...,N). \tag{9}$$

It is convenient to note here a special feature of the Sadovskii vortex for which W is the plane $y=0$. It is clear that in this case we can fix B because of scale invariance due to the absence of a natural length, so that we have lost the unknown x_N. (There is similarity of solutions with the same value of $U/\omega l$, $l = x_N - x_0$.) However, the net force on S in the x direction must vanish in this case, so

$$\int_{x_0}^{x_n} p \frac{dy}{dx}\, dx = 0, \tag{10}$$

leading to

$$\sum_{S=1}^{N-1} (y_{s+1} - y_{s-1}) R_s = 0, \tag{11}$$

so that the Eqs. (8) are not independent. We could simply drop one equation but more satisfactory methods for dealing with the difficulty exist and are described in Sec. III F.

An interesting property of the solution, noticed by Chernyshenko[8] and Smith,[7] is that once a solution has been found either U or ω, or both, can have its sign changed without changing the geometry. This is because ψ_- is proportional to ω and independent of U and ψ_+ is proportional to U and independent of ω, while (3) involves only squared terms.

B. Flow near separation and reattachment

We consider the flow in the interior region close to the separation point A. The equation to determine ψ_- takes on the approximate form

$$\frac{\partial^2 \psi}{\partial y^2} = -\omega, \tag{12}$$

so that the particular integral $\psi_-^{(p)}$ is approximately

$$\psi_-^{(p)} = -\tfrac{1}{2}\omega(y-y_A)^2 + \tfrac{1}{2}\omega(y-y_A)h(x-x_A), \tag{13}$$

where

$$y - y_A = h(x - x_A)$$

is the equation of S and $h(0)$, $h'(0)$ both vanish. Hence, as $x \to x_A$, q_- is $o(x-x_A)$ so that in view of (3)

$$q_+ = q + o[(x-x_A)^2]. \tag{14}$$

Locally, therefore, Kirchoffs' free streamline theory applies and it follows that

$$h(x-x_A) = a(x-x_A)^{3/2} + \cdots, \tag{15}$$

where a is a constant (Smith[10]).

We can easily determine higher terms in the particular integral; however, the complementary function $\psi_-^{(c)}$ is of a surprising form. By conformal mapping of the interior of the cusp into a half-plane, we can show

$$\psi_-^{(c)} = A \operatorname{Im} \exp[-(2\pi/a) z^{-1/2}] + \cdots, \tag{16}$$

where $z = (x-x_A) + i(y-y_A)$. This essential singularity has been overlooked in previous work. Its contribution is, however, exponentially small inside the patch, and it is therefore assumed that the expansions used below in Eqs. (18) and (22) for the shape and strength of the vortex sheet do not need to recognize its presence explicitly.

III. TWO METHODS OF SOLUTION

In this section we describe two different methods of calculating the Sadovskii vortex and the rotational corner flow.

The first method represents the velocity at any point of S as a sum of contributions from the vortex sheet and its image in W and from the constant vorticity patch P and its image in W; the latter being expressed as a contour integral around the boundary of the patch. This method, which is described in Secs. III A–III D, works for any boundary W for which the image function for a point vortex is known. Its disadvantage is that it does not exploit the linearity of the problem of finding the velocity field for given S and W and this leads to a final system of algebraic equations roughly twice the size of that described in Sec. II.

The second method is more in the spirit of Sec. II in that the problem is split into a linear part—solved by a boundary-integral method—and a nonlinear part, essentially that described in Sec. II. A drawback of this method is that the calculation of the Jacobian for solution by Newton's method is expensive.

We choose to describe the methods in the context of the Sadovskii vortex and to relegate the algebraic details of the corner flow to the Appendix. The geometrical description of S, which is common to both methods, is described first.

A. Parametrization of S

We can choose the coordinates of A to be (1,0), those of B to be (−1,0), and choose U to be (1,0); see Fig. 2(a). We introduce θ by

$$x = -\cos\theta \tag{17}$$

and parametrize S by writing

$$y(\theta) = \sin^3\theta \sum_{n=0}^{\infty} a_n \cos n\theta. \tag{18}$$

Thus we have built into our parametrization the requirement (15), with the objective of enhancing the convergence of the cosine series. Sadovskii[3] overlooked (15), claiming S had finite curvature at A and B, while Smith[7] did not impose (15), but used it as a consistency check. Note that (18) does not impose any symmetry constraints.

For the corner flow [Fig. 2(b)] we choose A to be (1,0), B to be (0,h), and $\psi = -xy$ at infinity. We define $\hat{x}$ and $\hat{y}$ by

$$x + iy = \sqrt{\hat{x} + i\hat{y}} \tag{19}$$

and introduce θ by

$$\hat{x} = \tfrac{1}{2}[(1-h^2) - (1+h^2)\cos\theta]. \tag{20}$$

Then we build in the requirement (15) by the representation

$$\hat{y} = \sin^3\theta \sum_0^\infty a_n \cos n\theta. \tag{21}$$

This parametrization is suggested by the conformal map of a half-plane into a corner and this method of constructing a suitable parametrization of S can be extended to other geometries.

B. A vortex-sheet method

We suppose the vortex sheet has strength $\gamma(\theta)$ and represent it as a cosine series

$$\gamma(\theta) = \sum_0^\infty b_n \cos n\theta. \tag{22}$$

Then the complex velocity $Q^{(1)}$ at a point $z(\theta)$ of the sheet due to the sheet and its image in $y=0$ is

$$Q^{(1)}_{\pm}(\theta) = \mp\tfrac{1}{2}\frac{G(\theta)}{(dz/d\theta)} - \frac{i}{2\pi}\int_0^\pi \frac{G(\theta')d\theta'}{z(\theta)-z(\theta')} + \frac{i}{2\pi}\int_0^\pi \frac{G(\theta')d\theta'}{z(\theta)-\bar{z}(\theta')}, \tag{23}$$

where "+" denotes, as before, the exterior of S and "−," the interior and

$$z(\theta) = -\cos\theta + iy(\theta),$$

where $y(\theta)$ is given by Eq. (18) and where

$$G(\theta) = \gamma(\theta)\left|\frac{dz}{d\theta}\right|. \tag{24}$$

The first integral is the contribution due to the sheet itself and is a Cauchy principal value.

The complex velocity $Q^{(2)}$ due to the uniform vorticity in ρ and its image in $y=0$ can be expressed as a line integral over ∂P by the method of contour dynamics, a form very convenient for computation being due to Pullin.[11] Application of his method leads to

$$Q^{(2)} = -\frac{\omega}{4\pi}\int_0^\pi \left(\frac{\bar{z}(\theta)-\bar{z}(\theta')}{z(\theta)-z(\theta')}\frac{dz}{d\theta}(\theta') + \frac{z(\theta)-z(\theta')}{z(\theta)-\bar{z}(\theta')}\frac{d\bar{z}}{d\theta}(\theta')\right)d\theta' + K(\theta), \tag{25}$$

where

$$K(\theta) = (\omega/4\pi)[\bar{z}(\theta)-z(\theta)]\{\ln[z(\theta)+1] - \ln[z(\theta)-1]\} + \omega/\pi \tag{26}$$

is the contribution to the line integral from the interval $(-1,1)$.

We define the total velocity Q by

$$Q_{\pm}(\theta) = Q^{(1)}_{\pm}(\theta) + Q^{(2)}(\theta) - 1 \tag{27}$$

and the problem is to choose the infinite set of constants $\{a_r, b_s, q\}$ so that

$$|Q_+(\theta)|^2 - |Q_-(\theta)|^2 = q^2 \quad (0 \leqslant \theta \leqslant \pi) \tag{28}$$

and

$$\mathrm{Im}\left(Q_+(\theta)\frac{dz}{d\theta}\right) = 0 \quad (0 \leqslant \theta \leqslant \pi). \tag{29}$$

Equation (29) ensures that S is a streamline; it follows from (23) that (29) ensures

$$\mathrm{Im}\left(Q_-(\theta)\frac{dz}{d\theta}\right) = 0. \tag{30}$$

We decided to compute first the symmetric solutions reported by both Sadovskii[3] and Smith.[7] Thus we set to zero a_{2s+1} and b_{2s+1} $(s=0,1,2,\ldots)$. Next we truncated the system by satisfying (28) and (29) only at a finite set of points θ_s where

$$\theta_s = s\pi/(2N) \quad (s=0,1,\ldots,N). \tag{31}$$

However, (29) is automatically satisfied at $\theta=0$ and $\theta=\pi/2$ so that the discrete system becomes

$$|Q_+(\theta_s)|^2 - |Q-(\theta_s)|^2 = q^2 \quad (s=0,1,\ldots,N) \tag{32}$$

and

$$\mathrm{Im}\left(Q_+(\theta_s)\frac{dz}{d\theta}(\theta_s)\right) = 0 \quad (s=1,2,\ldots,N-1), \tag{33}$$

a total of $2N$ equations. We must now truncate the series (18) and (22) so as to produce the correct number of unknowns. There are no general rules to guide us in this process. Now if we fix the shape and consider the subproblem in which (33) determines the vortex-sheet strength γ we are obliged to retain exactly the set $b_0, b_2, \ldots, b_{2(N-2)}$. We decided to retain the same set in the full problem, forcing us to take our vector u of unknowns to be the $2N$ vector

$$u = (a_0, a_2, \ldots, a_{2(N-1)}, b_0, b_2, \ldots, b_{2(N-2)}, q). \tag{34}$$

Equations (32) and (33) can be written

$$F(u,\omega) = 0, \tag{35}$$

which, for given ω, can be solved by Newton's method. Once solved, ω provides a convenient continuation parameter. The Jacobian matrix, which is $2N \times 2N$, was found numerically.

C. Evaluation of the integrals

The integrals (23) and (25) were evaluated by Simpson's rule, using M ordinates equally spaced in θ, where M is independent of N. This flexibility is valuable because it enables us to cope with the difficulties which arise at the ends of the range of integration, where S is cusped.

The integrand of the first integral is infinite at $\theta=\theta'$ and the integral must be interpreted as a Cauchy principal value. The integrand of the second integral is finite but assumes large values when $\theta \sim \theta'$ and $\theta' \ll 1$ or $\pi - \theta' \ll 1$. The second term in the integrand in (25) is bounded but rapidly varying in the cusp region since

$$\frac{z(\theta)-z(\theta')}{z(\theta)-\bar{z}(\theta')} = \frac{r_1}{r_2}e^{i(\alpha-\beta)}, \tag{36}$$

where r_1, r_2, α, and β are defined in Fig. 3. The first term is well behaved. We can suppress the difficulty at the cusps by choosing M to be large enough. We require, at the first collocation point θ_1,

$$r(\theta_1) = y(\theta_1)/\Delta x(\theta_1) \geqslant r_c, \tag{37}$$

where $\Delta x(\theta)$ is the spacing of the *integration* mesh points and r_c is a constant of order unity (cf. Maskew[12]) which leads to the requirement

$$M \geqslant 8\sqrt{2} r_c N^2/\pi a. \tag{38}$$

We can take $r_c = 1$ and $a = 1$ for illustrative purposes. Then we see that the restriction can be satisfied in practice for moderate N but at $N = 60$ it would require $M \geqslant 12\,963$, which is impracticable.

Thus we decided to improve the behavior of the integrands by use of cancellation. For example, expansion of the numerator and denominator of the integrand of the second integral in (23) shows that, when $\theta \sim \theta'$,

$$\frac{G(\theta')}{z(\theta) - \bar{z}(\theta')} \cong \left(G(\theta) + (\theta' - \theta)\frac{dG}{d\theta}(\theta)\right)\left(2iy(\theta) - (\theta' - \theta)\frac{d\bar{z}}{d\theta}(\theta) - \frac{1}{2}(\theta' - \theta)^2 \frac{d^2\bar{z}}{d\theta^2}(\theta)\right)^{-1}. \tag{39}$$

Since $G(\theta) = O(\theta), x(\theta) = O(\theta^2)$, and $y(\theta) = O(\theta^3)$, the integrand is $O(\theta^{-2})$ when $\theta \ll 1$. Note also that the terms retained in each expansion are comparable when $\theta' = O(\theta)$ and $\theta \ll 1$. We observe that the right-hand side of (39) can be integrated with respect to θ' in closed form, as can the similar expansions

$$\frac{G(\theta')}{z(\theta) - z(\theta')} \cong \left(G(\theta) + (\theta' - \theta)\frac{dG}{d\theta}\right)\left(-(\theta' - \theta)\frac{dz}{d\theta} - \frac{1}{2}(\theta' - \theta)^2 \frac{d^2 z}{d\theta^2}\right)^{-1} \tag{40}$$

and

$$\frac{z(\theta) - z(\theta')}{z(\theta) - \bar{z}(\theta')}\frac{d\bar{z}}{d\theta}(\theta') \cong -\left((\theta' - \theta)\frac{dz}{d\theta} + \frac{1}{2}(\theta' - \theta)^2 \frac{d^2 z}{d\theta^2}\right)\left(\frac{d\bar{z}}{d\theta} + (\theta' - \theta)\frac{d^2\bar{z}}{d\theta^2}\right) \times \left(2iy(\theta) - (\theta' - \theta)\frac{d\bar{z}}{d\theta} - \frac{1}{2}(\theta' - \theta)^2 \frac{d^2\bar{z}}{d\theta^2}\right)^{-1}, \tag{41}$$

where all derivatives are evaluated at θ. We thus used these expansions as cancellation functions, integrating the difference between the left-hand and right-hand sides of (39), (40), and (41) by Simpson's rule and integrating the remainder term analytically.

D. Tests of the method

It is easy to construct analytic solutions in which S is an arc of a circle (of course, these are not steady) and these solutions were used for initial testing of the subroutines which evaluated the integrals. The only exact solution in which S has cusps that we could find was the corner flow with $\omega = 0$ for which a routine application of Kirchhoff's free-streamline theory gives $q = \frac{3}{4}$ and for S the equation

$$x^{2/3} + y^{2/3} = 1; \tag{42}$$

straightforward algebra shows that

$$a_n = \frac{(2 - \delta_{n0})}{4\pi}\int_0^{\pi} \cos n\theta \frac{\sin^3\psi(\theta)}{\sin^3\theta}\, d\theta, \tag{43}$$

where $\psi(\theta)$ is defined by the requirement $0 \leqslant \psi \leqslant \pi$ and

$$\cos 3\psi + 15\cos\psi = 16\cos\theta \quad (0 \leqslant \theta \leqslant \pi). \tag{44}$$

Table I shows the results obtained when cancellation is applied to the first integral in (23) only, to deal with the principal value. In the table, r is as defined in (37), $p = q_+^2 - q_-^2 - q^2$, and n is the component of the velocity normal to S. Thus $p = n = 0$ in the exact solution, so the computed values are a measure of the numerical error. Evidently, the velocity is very inaccurate when $r \ll 1$, but improves as $r \sim 1$, as anticipated in the previous section. Table II shows the results when cancellation is applied to both integrals in (23). The improvement for $r \ll 1$ is very marked, although some loss of accuracy is evident due, presumably, to imperfect cancellation.

Unfortunately, we have no test of the cancellation method for $\omega \neq 0$.

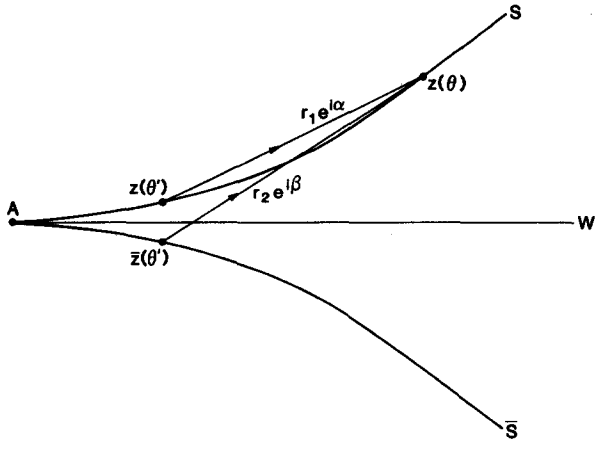

FIG. 3. Sketch defining the symbols in Eq. (36).

E. An alternative formulation

Instead of solving for the location and strength of the vortex sheet simultaneously, one can formulate the calculation so that first the kinematic problem is solved for the velocity with an assumed shape and then the shape is iterated until the pressure condition is satisfied. We describe the

TABLE I. $N = 30$ and (a) $M = 241$, (b) $M = 481$. Cancellation is applied to the first integration (23) only. Here p is the pressure residual, n is the normal velocity residual, and r is the ratio defined in (37).

		(a)		
x	y	r	p	n
0.000 009 77	0.999 314 53	0.0285	−0.16E + 01	0.25E − 01
0.000 078 24	0.997 257 19	0.1142	−0.11E + 00	−0.87E − 03
0.000 264 53	0.993 825 14	0.2573	0.31E − 01	−0.33E − 02
0.000 628 55	0.989 013 65	0.4585	0.18E − 01	−0.50E − 03
0.001 231 48	0.982 816 03	0.7187	0.42E − 02	0.25E − 03
0.002 136 16	0.975 223 60	1.0389	0.60E − 03	0.12E − 03
0.003 407 66	0.966 225 67	1.4205	0.55E − 04	0.23E − 04
0.005 113 69	0.955 809 40	1.8653	0.29E − 05	0.25E − 05
0.007 325 27	0.943 959 84	2.3751	0.37E − 07	0.16E − 06
0.010 117 30	0.930 659 85	2.9523	−0.90E − 08	0.40E − 08
		(b)		
x	y	r	p	n
0.000 009 77	0.999 314 53	0.0570	−0.56E + 00	0.68E − 02
0.000 078 24	0.997 257 19	0.2283	0.27E − 01	−0.26E − 02
0.000 264 53	0.993 825 14	0.5146	0.13E − 01	−0.83E − 04
0.000 628 55	0.989 013 65	0.9171	0.12E − 02	0.12E − 03
0.001 231 48	0.982 816 03	1.4374	0.47E − 04	0.14E − 04
0.002 136 16	0.975 223 60	2.0778	0.72E − 06	0.52E − 06
0.003 407 66	0.966 225 67	2.8411	0.11E − 08	0.67E − 08
0.005 113 69	0.955 809 40	3.7305	−0.54E − 09	−0.38E − 09
0.007 325 27	0.943 959 84	4.7501	−0.38E − 09	−0.24E − 09
0.010 117 30	0.930 659 85	5.9046	−0.30E − 09	−0.13E − 09

method in the context of the Sadovskii problem and then outline the modifications for the corner in the Appendix.

We employ Cauchy's integral theorem to relate the velocity at a point on S to an integral around the boundary of the vortex and its image in the x axis. The formulation is similar to that used by Tanaka *et al.*[13] for unsteady water wave calculations. Consider first the external velocity. Applying the integral theorem to $Q(z')/(z'-z)$, which is analytic in the external region, and using the indented contour shown in Fig. 4, we have

$$-\pi i Q + \int_{s+\bar{s}} \frac{Q'\,dz'}{z'-z} = \int_{\infty} \frac{Q'\,dz'}{z'-z}, \tag{45}$$

where both integrals are taken in the clockwise sense, and the integral on the left-hand side is to be interpreted as a Cauchy principal value. As before, Q denotes the complex velocity $u - iv$.

The integral at infinity is $2\pi i U$, where U is positive when the flow is from right to left. Consider now the integral around the vortex and its image. Let ϕ and ψ denote the velocity potential and streamfunction in the external region. On the boundary, $\psi = \text{const}$ and so

$$Q\frac{dz}{d\theta} = \frac{d\phi}{d\theta} + i\frac{d\psi}{d\theta} = \frac{d\phi}{d\theta}. \tag{46}$$

Multiply (45) by $dz/d\theta$ and take the imaginary part. We obtain

$$-\frac{d\phi}{d\theta} + \frac{1}{\pi}\int_0^{\pi} \frac{d\phi}{d\theta}(\theta')\,\mathrm{Im}\left(\frac{dz/d\theta}{z(\theta')-z(\theta)}\right)d\theta' - \frac{1}{\pi}\int_0^{\pi} \frac{d\phi}{d\theta}(\theta')\,\mathrm{Im}\left(\frac{dz/d\theta}{\bar{z}(\theta')-z(\theta)}\right)d\theta' = 2U\frac{dx}{d\theta}, \tag{47}$$

where we have converted the contour integral into line integrals, exploiting the symmetry about the x axis.

Given the shape of the vortex $z(\theta)$, Eq. (47) is a Fredholm integral equation of the second kind for the unknown function $d\phi/d\theta$. When this is found, the velocity follows from (46). Note that the integrand in the first integral is not singular at $\theta = \theta'$ as $\lim_{\theta' \to \theta}\{(dz/d\theta)/[z(\theta') - z(\theta)]\}$ is real.

TABLE II. $N = 30$ and (a) $M = 241$, (b) $M = 481$. Full cancellation is applied in Eq. (23). Here p, n, and r are as before.

		(a)		
x	y	r	p	n
0.000 009 77	0.999 314 53	0.0285	−0.50E − 05	−0.25E − 05
0.000 078 24	0.997 257 19	0.1142	0.11E − 07	0.31E − 06
0.000 264 53	0.993 825 14	0.2573	0.24E − 06	0.31E − 05
0.000 628 55	0.989 013 65	0.4585	−0.14E − 05	0.97E − 06
0.001 231 48	0.982 816 03	0.7187	−0.13E − 05	−0.64E − 06
0.002 136 16	0.975 223 60	1.0389	−0.46E − 06	−0.50E − 06
0.003 407 66	0.966 225 67	1.4205	−0.74E − 07	−0.15E − 06
0.005 113 69	0.955 809 40	1.8653	−0.11E − 07	−0.27E − 07
0.007 325 27	0.943 959 84	2.3751	−0.97E − 08	−0.36E − 08
0.010 117 30	0.930 659 85	2.9523	−0.88E − 08	−0.11E − 08
		(b)		
x	y	r	p	n
0.000 009 77	0.999 314 53	0.0570	−0.31E + 06	−0.70E − 06
0.000 078 24	0.997 257 19	0.2283	0.13E − 06	0.10E − 05
0.000 264 53	0.993 825 14	0.5146	−0.39E − 06	0.99E − 07
0.000 628 55	0.989 013 65	0.9171	−0.17E − 06	−0.21E − 06
0.001 231 48	0.982 816 03	1.4374	−0.13E − 07	−0.41E − 07
0.002 136 16	0.975 223 60	2.0778	−0.13E − 08	−0.27E − 08
0.003 407 66	0.966 225 67	2.8411	−0.14E − 08	−0.20E − 09
0.005 113 69	0.955 809 40	3.7305	−0.10E − 08	−0.11E − 09
0.007 325 27	0.943 959 84	4.7501	−0.75E − 09	−0.84E − 10
0.010 117 30	0.930 659 85	5.9046	−0.57E − 09	−0.63E − 10

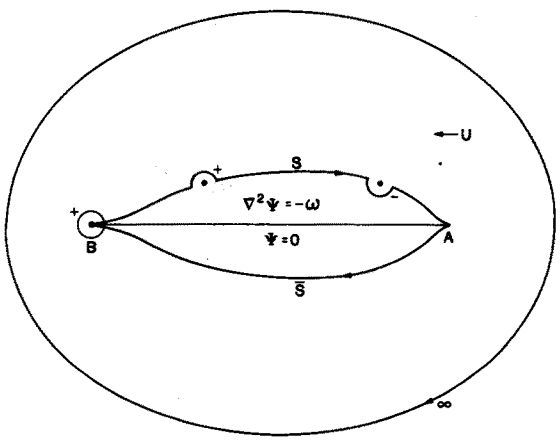

FIG. 4. The contours for the application of Cauchy's theorem, the indentations at + and − being used for the exterior and interior velocity. Note the special form of + at B.

The solution of (47) is not altogether straightforward because of the cusp. We have that $d\phi/d\theta$ vanishes like θ (or $\pi-\theta$) at the cusps, since $dz/d\theta \sim \theta$ (or $\pi-\theta$) and the velocity is finite. Then the integrands in (47) are bounded when $z=\pm 1$, and the equation is satisfied identically at the ends. We can, however, obtain an equation satisfied at the end points by evaluating (45) at the end points, with an extra factor 2 in front of the first term because the indentation should then be a complete circle, as shown in Fig. 3. This gives the equation

$$-u_{\pm 1}-\frac{1}{\pi}\int_0^{\pi} y\,\frac{d\phi}{d\theta}\,\frac{d\theta}{|z\mp 1|^2}=U. \tag{48}$$

Since $y=O(\theta^3)$, the integrand has a finite limit at $z=1$, and similarly at the other cusp.

The procedure adopted to solve (47) was to write

$$\frac{d\phi}{d\theta}=\sin\theta\sum_0^N c_n^+\cos n\theta, \tag{49}$$

and satisfy (47) at the points $\theta_j=j\pi/N, j=1,\ldots,N-1$, and (48) at the ends. This gives a linear system of $N+1$ equations for the $N+1$ unknowns $c_0^+,\ldots,c_N^1$, which were solved using a standard linear solver. The integrals were evaluated by Simpson's rule at $M>N$ points. The value of M was chosen sufficiently large to ensure accuracy at the end points. Cancellation as described in Sec. III C was not employed, as calculations using this formulation were employed just to check the first method and test for bifurcation into nonsymmetric solutions.

We now consider the interior velocity. Let Ψ be any solution of

$$\nabla^2\Psi=-\omega \quad (y>0), \quad \Psi=0 \quad \text{on } y=0, \tag{50}$$

inside the vortex. Then the interior velocity components are $(u+\partial\Psi/\partial y, v-\partial\Psi/\partial x)$, where $u-iv$ is analytic in the interior, and has a complex potential $\phi+i\psi$. We continue $u-iv$ and Ψ analytically across $y=0$. The continuation is given by

$$\begin{aligned} &u(x,y)=u(x,-y), \quad v(x,y)=-v(x,-y),\\ &\Psi(x,y)=-\Psi(x,-y). \end{aligned} \tag{51}$$

Applying Cauchy's integral theorem to the contour around the vortex and its image as shown in Fig. 3, and repeating the steps leading to (47) for the exterior velocity, we obtain

$$\begin{aligned} &\frac{d\phi}{d\theta}+\frac{1}{\pi}\int_0^{\pi}\frac{d\phi}{d\theta}(\theta')\,\mathrm{Im}\left(\frac{dz/d\theta}{z(\theta')-z(\theta)}\right)d\theta'\\ &\quad-\frac{1}{\pi}\int_0^{\pi}\frac{d\phi}{d\theta}(\theta')\,\mathrm{Im}\left(\frac{dz/d\theta}{\bar z(\theta')-z(\theta)}\right)d\theta'\\ &=-\frac{1}{\pi}\int_0^{\pi}\frac{d\psi}{d\theta}(\theta')\mathrm{Re}\left(\frac{dz/d\theta}{z(\theta')-z(\theta)}\right)d\theta'\\ &\quad-\frac{1}{\pi}\int_0^{\pi}\frac{d\psi}{d\theta}(\theta')\mathrm{Re}\left(\frac{dz/d\theta}{\bar z(\theta')-z(\theta)}\right)d\theta'. \end{aligned} \tag{52}$$

Since the boundary of the vortex is a streamline,

$$\psi=-\Psi \quad \text{on } S. \tag{53}$$

Hence the right-hand side is a known function of θ, and we again have a Fredholm integral equation for $d\phi/d\theta$ in the interior.

The evaluation of the left-hand side of (52) proceeds away from the cusps as for the exterior calculation. The right-hand side is more difficult. We can remove the principal value integral by adding and subtracting $d\psi/d\theta$ multiplied by the integral of

$$\mathrm{Re}\left(\frac{(dz/d\theta)(\theta')}{z(\theta')-z(\theta)}\right),$$

which can be evaluated exactly. This gives for the right-hand side, using (53),

$$\begin{aligned} &\frac{1}{\pi}\int_0^{\pi}\left[\frac{d\psi}{d\theta}(\theta')\mathrm{Re}\left(\frac{(dz/d\theta)(\theta)}{z(\theta')-z(\theta)}\right)\right.\\ &\quad\left.-\frac{d\psi}{d\theta}(\theta)\mathrm{Re}\left(\frac{(dz/d\theta)(\theta')}{z(\theta')-z(\theta)}\right)\right]d\theta'\\ &\quad+\frac{1}{\pi}\frac{d\psi}{d\theta}\ln\left|\left(\frac{1-z(\theta)}{1+z(\theta)}\right)\right|\\ &\quad+\frac{1}{\pi}\int_0^{\pi}\frac{d\psi}{d\theta}(\theta')\mathrm{Re}\left(\frac{(dz/d\theta)(\theta)}{\bar z(\theta')-z(\theta)}\right)d\theta'. \end{aligned} \tag{54}$$

The integrands are now bounded for $z\neq\pm 1$.

To obtain equations satisfied at the ends, we repeat the procedure which led to (48) to obtain, analogous to (48),

$$\int_0^{\pi} y\,\frac{d\phi}{d\theta}\,\frac{d\theta}{|z\mp 1|^2}=-\int_0^{\pi}\frac{(x\mp 1)}{|z\mp 1|^2}\,\frac{d\Psi}{d\theta}\,d\theta. \tag{55}$$

The equation for the interior value of $d\phi/d\theta$ was solved by writing

$$\frac{d\phi}{d\theta}=\sin\theta\sum_0^N c_n^-\cos n\theta \tag{56}$$

and satisfying (52) at the $N-1$ points $\theta_j=j\pi/N$, $j=1,\ldots,N-1$. The integrals were again evaluated using Simpson's rule using M integration points. Two further equations follow from (55) giving $N+1$ linear equations for the $N+1$ unknown c_n^-.

Note that it is advantageous if Ψ can be found to satisfy the symmetry conditions, but it is not necessary. One can restrict the Cauchy integral to the boundary of the vortex for any Ψ, in which case one obtains an integral equation for $d\phi/d\theta$ around the entire boundary, and not just on the vortex sheet S.

F. The counting problem

Having found c_n^- and c_n^+, we have the velocity on each side of the vortex sheet and the residual function

$$R(\theta)=q_+^2-q_-^2-q^2 \tag{57}$$

is determined. The procedure now is to iterate on the shape until $R(\theta)=0$ to an acceptable accuracy.

We turn now to the counting question for this formulation. We employed $N-1$ interior collocation points $\theta_j=j\pi/N$ ($j=1,2,\ldots,N-1$) for the calculation of the velocity. There are therefore $N-1$ arbitrary y coordinate values, these being the value of y at the interior collocation

points. It is thus appropriate to truncate (18) and hence to represent the shape by $N-1$ coefficients a_n,

$$y=\sin^3\theta\sum_0^{N-2} a_n\cos n\theta \quad (0\leqslant\theta\leqslant\pi). \tag{58}$$

For the unknown coefficients a_n, we have $N+1$ equations

$$R(\theta_j)=0, \quad j=0,1,...,N. \tag{59}$$

In addition, if we take $U=1$ and regard c_2 $[=\frac{1}{2}(1-q^2)]$ as given, there is a further unknown ω. Thus we have $N+1$ equations for N unknowns, leading to a mismatch.

Notice that the counting problem disappears if we assume fore–aft symmetry. Take N to be even so that there is a collocation point at the midpoint. There are $N/2+1$ equations from the vanishing of R at $j=0,1,...,N/2$, and $N/2$ coefficients a_{2m} $[0\leqslant m\leqslant N/2-1]$ for $N/2y$ coordinates. Including ω, the number of equations equals the number of unknowns.

The reason for the mismatch, as discussed earlier, is that Eqs. (59) are not independent, because of the zero drag condition (10), which leads to

$$\sum_0^N R(\theta_j)\frac{dy_j}{d\theta}=0. \tag{60}$$

It is clear that (60) is no problem when the shape is assumed symmetrical as we only satisfy the equations over the front or back of the sheet. A similar problem was encountered by Chen and Saffman[14] in their attempt to calculate nonsymmetrical finite amplitude water waves of permanent form. One way to proceed is simply to discard one of the equations (62). This has the disadvantage that it is not clear which equation should be dropped. [Experience with water waves where N was commonly $O(10^3)$ showed that dropping one equation transformed an ill-posed problem into a nearly singular one, so that the Jacobian was very small and convergence to a solution was difficult.]

Chen and Saffman overcame the difficulty by a trick suggested by the Lagrange undetermined multipliers method for finding stationary values subject to constraints. The system (59) is inflated to the system

$$R(\theta_j)+\lambda f(\theta_j)=0, \quad j=0,1,...,N, \tag{61}$$

where $f(\theta)$ is completely arbitrary subject to the constraint that

$$\int_0^\pi f(\theta)\frac{dy}{d\theta}\,d\theta\neq 0. \tag{62}$$

With λ as a further unknown, we have $N+1$ equations for the $N+1$ unknowns $a_0,a_1,...,a_{N-2},\omega,\lambda$. We now choose $f(\theta)$ so that the Jacobian of (61) is nonsingular. Then the solution of the system is isolated, and if it has $\lambda=0$, we then have a unique solution of our system (59). The method is not infallible. If (49) has a solution then there must be a solution of the inflated system (61) with $\lambda=0$, but there is no guarantee that an iterative method will find this solution. In practice, however, the method seems to work well and choosing $f=\theta-\pi/2$ led to solutions with $\lambda\sim O(10^{-10})$.

We used Newton's method to solve the system, using as a first guess one of the symmetrical solutions found by the vortex-sheet method. We checked the eigenvalues of the Jacobian matrix to see if there were any bifurcation points. None were found and it seems that the Jacobian is never singular in the range of ϵ studied. The calculations indicate that the symmetrical solutions found by the vortex-sheet method are unique, or at least if there is another family of solutions they do not joint continuously with the calculated branch. The present method is expensive because it is necessary to calculate the velocities of a perturbed shape to find each row of the Jacobian, and without use of a cancellation technique to reduce the oscillations of the integrands in the integral equations for $d\phi^{\pm}/d\theta$, it was necessary to use $M\sim 4000$ when $N\sim 32$, which made the evaluation of the integrals time consuming. For $c_2=0.2$, we obtained $\omega=10.4771$, $y_{\max}=0.247\,15$, to be compared with the values in Table III, which gives the results of the vortex-sheet method.

IV. RESULTS FOR THE SADOVSKII VORTEX

In this section we describe the results obtained for the Sadovskii vortex using the methods described in Sec. III. Method 1 was used to obtain values of the parameters describing the Sadovskii vortex, method 2 then being used as a check.

We decided to facilitate comparison with Smith's[7] work by fixing the constant q and regarding ω as an unknown and replacing q itself by his parameter c_2, defined by

$$c_2=\tfrac{1}{2}(1-q^2). \tag{63}$$

In this notation, the slender limit discussed by Childress[2] is $c_2\to 0$ while the limit $q=0$ corresponds to $c_2=0.5$.

A. Convergence

We decided to study the case $c_2=0.2$ in detail so that we could satisfy ourselves that method 1 converged as N, the number of collocation points, increased and to provide detailed numerical results to aid future researchers to compare with us. Table III shows the results for $N=32$, 64, and 97. ($N=96$ was intended, but an error was made. The run was not repeated because of cost.) The number of integration points M was set at 961, 1921, and 2911, respectively. Evi-

TABLE III. Results for $c_2=0.2$. Here y_m is the height of the vortex at the midpoint $x=0$, a is defined in Eq. (11), and er is $|q-\gamma(\pm 1)|$, which is zero in the exact solution [Eq. (7)] $M=961$, 1921, and 2911 when $N=32$, 64, and 97.

	$N=32$	$N=64$	$N=97$
y_m	0.247 133 3465	0.247 133 3513	0.247 133 3516
ω	10.477 718 25	10.477 718 06	10.477 718 04
$\gamma(\pm 1)$	0.774 715	0.774 658	0.774 641
a	0.255 689	0.255 704	0.255 709
er	0.000 12	0.000 061	0.000 045

dently the method is converging, more rapidly for the gross quantities y_m and ω than for $\gamma(\pm 1)$ and a, which are quantities associated with the cusp. This is confirmed by the values of er defined by

$$er = |q - \gamma(\pm 1)|, \tag{64}$$

which is zero in the exact solution, according to Eq. (7) (note $\gamma < 0$ in Sec. II). It appears that er gives a good estimate of the error in resolving the cusp, but that the error in y_m and ω is much smaller. Moreover er is roughly proportional to N^{-1}, suggesting that only a modest increase in resolution of the cusp is being achieved. This was confirmed by running the test code of Sec. III D with the same parameters. The error in the normal velocity at the first collocation point decreased only slowly, being 0.86×10^{-6}, 0.33×10^{-6}, and 0.61×10^{-7} when $N = 32$, 64, and 97, respectively. The critical spacing ratio r, defined in Eq. (37), has the values 0.1, 0.05, and 0.03 in the three cases and this decrease probably accounts for the comparative lack of improvement when N is increased. It is not feasible to increase M sufficiently to keep r constant [cf. Eq. (38)].

Table IV gives the first 15 Fourier coefficients computed with $N = 97$; when $N = 64$ the results differed by at most 2×10^{-6}. This is of the order of magnitude of the errors which the above discussion suggests will arise in computing the velocity field in the cusp region. Graphical examination of the first 15 coefficients shows that they decay roughly exponentially.

B. Properties of the Sadovskii vortex

Figure 5 shows a comparison with previous work. There is a discrepancy of about 10% with Smith's[7] values of $\omega(c_2)$, whereas we agree with Sadovskii[3] to graphical accuracy, except for the limiting case $c_2 = 0.5$. The slender body theory of Childress[2] gives values too low in this range of c_2; even when $c_2 = 0.025$, the discrepancy is still more than 5%. We will return to this point later. Values of y_m (ω) agree better with those given by Smith,[7] the discrepancy being less than 2%.

Figures 6 and 7 give profiles of $y(x)$ and $\gamma(x)$ in the range $c_2 = 0.05(0.05).50$ and Table V gives the gross parameters in the range $0.025(0.025).475$. We believe the results are accurate to the number of figures shown.

TABLE IV. The first 15 Fourier coefficients as defined in Eqs. (18) and (22).

s	a_{2s}	b_{2s}
0	0.163 941	0.511 150
1	−0.084 854	0.304 507
2	0.006 914	−0.010 984
3	0.007 067	−0.035 181
4	−0.002 584	0.002 117
5	−0.000 590	0.005 546
6	0.000 614	−0.001 642
7	−0.000 001	−0.001 401
8	−0.000 137	0.000 519
9	0.000 025	0.000 277
10	0.000 029	−0.000 228
11	−0.000 011	−0.000 088
12	−0.000 006	0.000 063
13	0.000 004	0.000 010
14	0.000 001	−0.000 030

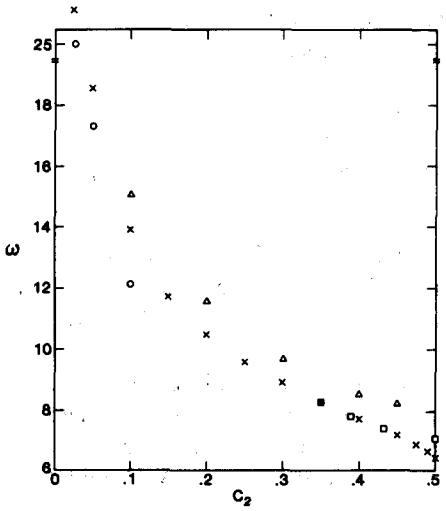

FIG. 5. A comparison with previous work for the function $\omega(c_2)$. Present work, ×; Childress, ⊙; Sadovskii, □; and Smith, △. Our value for $c_2 = 0.5$ is from Saffman and Tanveer.[5]

Two features of the results may be pointed out. First, the profiles are developing high curvature near $x = \pm 1$ and the sheet strength γ is developing a boundary layer at $x = \pm 1$ as $c_2 \to 0.5$, that is as $q \to 0$. This reflects the fact that, as noticed by Chernyshenko[8] and Smith,[6] $q \to 0$ is a singular limit. The reason for this behavior is that, as shown by Saffman and Tanveer,[5] the profile of the no vortex-sheet limit intersects $y = 0$ orthogonally. To achieve this limit the cusp region of the Sadovskii vortex must shrink as $q \to 0$. Furthermore, γ is $O(q^2)$ for $x \neq \pm 1$ from Eq. (6) while Eq. (7) gives $\gamma(\pm) = q$, so that a boundary layer must form. To allow for this, we increased N from 40 to 75 for $c_2 = 0.45$ and

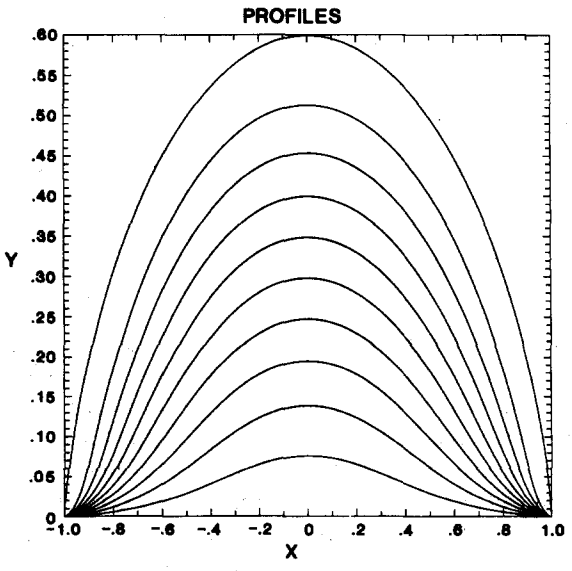

FIG. 6. Profiles $y(x)$ of the Sadovskii vortex for $c_2 = 0.05(0.05).5$, the last case being derived from Saffman and Tanveer. Note the magnification of the y coordinate. Here y_m (c_2) increases monotonically with c_2.

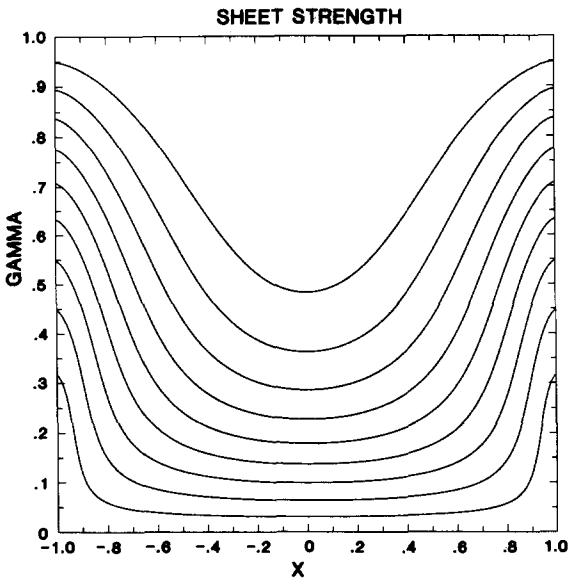

FIG. 7. Sheet strength $\gamma(x)$ for the Sadovskii vortex for $c_2 = 0.05(0.05).45$. $\gamma(\pm 1, c_2)$ decreases monotonically with c_2.

0.475. We return to the nature of the limit $q \to 0$ in the context of the corner flow, for which we have results for smaller values of q.

At the other extreme, we can see from Fig. 7 that considerable variation of $\gamma(x)$ remains when $c_2 = 0.05$, while the Childress[2] theory requires $\gamma(x) \approx 1$. This is consistent with our observation that the values of c_2 we considered are too large for the slender theory to hold.

The determinant of the Jacobian matrix and its smallest eigenvalue did not change sign in the range $0.05 \leqslant c_2 \leqslant 0.45$, so there are no bifurcations to solutions symmetric about $x = 0$. To test for bifurcations to nonsymmetric solutions, the Jacobian for the full problem in which the odd-order coefficients in the Fourier series are restored, was evaluated on the symmetric solution. A difficulty arises because of the constraint (11), which can be written

$$\sum_{s=0}^{M} L_s(u) F_s(u) = 0, \tag{65}$$

and the incompressibility condition

$$\int_0^{\pi} \mathrm{Im}\left(Q_+(\theta)\,\frac{dz}{d\theta}\right) d\theta = 0 \tag{66}$$

leading to

$$\sum_{s=0}^{M} K_s F_s(u) = 0, \tag{67}$$

where K_s are constants (equal to 1 or 0) and $L_s(u)$ is a linear function of u, L_s being zero if s corresponds to a normal velocity residual; M is the size of the full problem. Differentiating (65) and (67) with respect to u we find

$$\sum_{s=0}^{M} \left(\frac{\partial L_s}{\partial u_r} F_s + L_s \frac{\partial F_s}{\partial u_r}\right) = 0 \tag{68}$$

and

$$\sum_{s=0}^{M} K_s \frac{\partial F_s}{\partial u_r} = 0. \tag{69}$$

Thus K_s is a null vector of $\partial F/\partial u$ for all u and $L_s(u_0)$ is a null vector of $(\partial F/\partial u)|_{u_0}$, where u_0 is the symmetric solution, satisfying $F(u_0) = 0$.

We dealt with this simply by dropping a pressure and a normal velocity residual, to find that there were no bifurcations in $0.05 \leqslant c_2 \leqslant 0.45$.

TABLE V. Properties of the Sadovskii vortex. Here a is the cusp constant defined in Eq. (11) and er is the error estimate $|\gamma(\pm 1) - q|$.

n	c_2	ω	y_m	a	er
40	0.025	25.41	0.0399	0.026	0.33E − 04
40	0.050	18.56	0.0754	0.053	0.45E − 04
40	0.075	15.59	0.1079	0.082	0.55E − 04
40	0.100	13.83	0.1382	0.112	0.63E − 04
40	0.125	12.63	0.1669	0.144	0.71E − 04
40	0.150	11.74	0.1944	0.179	0.79E − 04
40	0.175	11.05	0.2211	0.216	0.88E − 04
40	0.200	10.48	0.2471	0.256	0.95E − 04
40	0.225	10.00	0.2727	0.300	0.10E − 03
40	0.250	9.58	0.2980	0.348	0.10E − 03
40	0.275	9.21	0.3232	0.402	0.10E − 03
40	0.300	8.87	0.3484	0.463	0.99E − 04
40	0.325	8.57	0.3738	0.534	0.93E − 04
40	0.350	8.28	0.3996	0.617	0.93E − 04
40	0.375	8.01	0.4260	0.719	0.55E − 04
40	0.400	7.74	0.4533	0.849	0.16E − 03
40	0.425	7.48	0.4820	1.026	0.31E − 04
75	0.450	7.21	0.5128	1.297	0.38E − 04
75	0.475	6.92	0.5476	1.832	0.13E − 04

V. RESULTS FOR THE ROTATIONAL CORNER FLOW

A. Properties of the solution

We reverted to the formulation of Sec. II and regarded the constant q as an unknown. The computed function $q(\omega)$ is shown in Fig. 8. The single value given by Chernyshenko[8] is in reasonable agreement with our results. Evidently $q \to 0$ as ω increases and a separate calculation of the $q = 0$ limiting case gave $\omega = 6.115\ldots$. Table VI gives the gross parameters

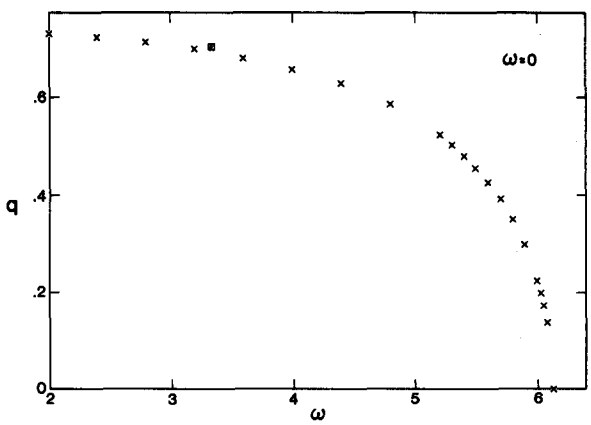

FIG. 8. The function $q(\omega)$ for the rotational corner flow. Present work, ×; Chernyshenko, ⊡. The value $q = \frac{1}{2}$ corresponds to $\omega = 0$.

TABLE VI. Properties of the rotational corner flow. Here s is the distance from the origin to the vortex sheet measured along the symmetry line $y = x$, and a and er are as before.

N	ω	q	s	a	er
40	0.500	0.7491	0.5014	0.546	0.92E − 04
40	1.000	0.7464	0.5056	0.550	0.92E − 04
40	1.500	0.7416	0.5128	0.557	0.92E − 04
40	2.000	0.7344	0.5231	0.568	0.92E − 04
40	2.500	0.7242	0.5367	0.583	0.91E − 04
40	3.000	0.7099	0.5541	0.605	0.90E − 04
40	3.500	0.6900	0.5758	0.637	0.89E − 04
40	4.000	0.6619	0.6028	0.683	0.85E − 04
40	4.250	0.6436	0.6187	0.715	0.83E − 04
40	4.500	0.6213	0.6364	0.754	0.80E − 04
40	4.750	0.5940	0.6564	0.806	0.76E − 04
40	5.000	0.5598	0.6790	0.874	0.70E − 04
40	5.250	0.5160	0.7051	0.970	0.64E − 04
40	5.500	0.4574	0.7358	1.118	0.60E − 04
40	5.750	0.3732	0.7735	1.385	0.52E − 04
46	6.000	0.2255	0.8262	2.17	0.37E − 03

as functions of q in the range $0.4 \leqslant \omega \leqslant 6.0$. Here, S is the distance of the sheet from the origin measured along the symmetry line $y = x$.

We had to increase resolution as $q \to 0$ for the reasons described in Sec. IV. With method 1, imposing symmetry with respect to the line $y = x$, $N = 4$ was adequate up to $\omega = 5.75$ but $N = 46$ was used to produce the tabular values at $\omega = 6.0$. A run at $\omega = 6.0$ with $N = 55$ diverged, possibly because of the extreme sensitivity of the solution in this region. A test run at $\omega = 5.3$ converged when $N = 31$ and $N = 46$ but diverged at $N = 61$, possibly for the same reason. We thus cannot assert that we have demonstrated convergence in this range of ω.

Figure 9 shows selected profiles, which again reveal the singular nature of the limit $q \to 0$. Figure 10 shows $\gamma(s)$ for

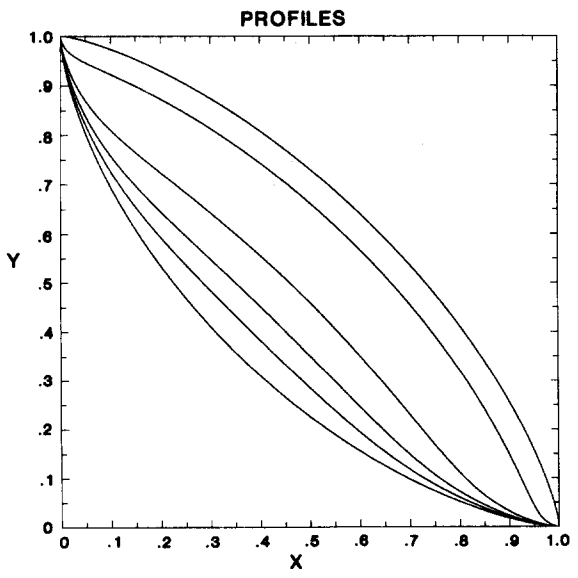

FIG. 9. The shape of the vortex sheet for $\omega = 0.5$, 3.0, 4.0, 5.0, 6.0, and 6.12..., the last value corresponding to $q = 0$. The distance to the sheet measured along $y = x$ increases monotonically with ω.

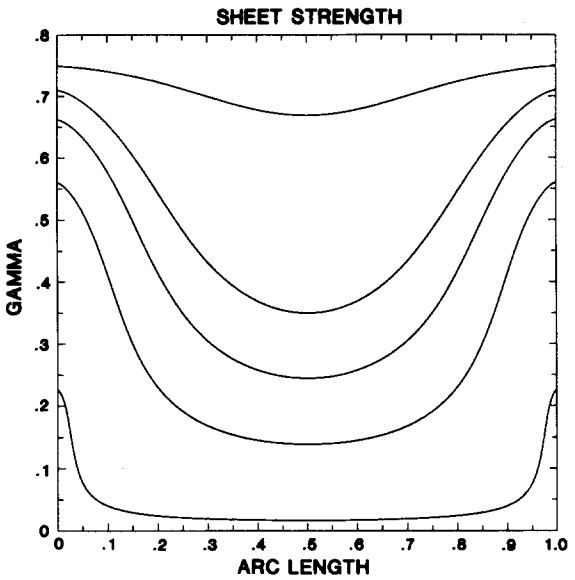

FIG. 10. The sheet strength $\gamma(s)$, where s is the arclength/net arclength.

the first five values of ω; s is arclength, divided by total arclength.

Method 2 was used without imposing symmetry. There is no analog of the constraint (11) so inflation was not needed. There were no bifurcations to other symmetric or nonsymmetric solutions.

B. Size of the cusp region as $q \to 0$

For $q \ll 1$, the solution must be close to that in the case $q = 0$, except very close to the attachment points A or B. It follows from the local analysis of the $q = 0$ case given by Saffman and Tanveer[5] that, near A,

$$q_+ \approx q_- \approx \omega \tilde{y} \ln|L/\tilde{y}|, \tag{70}$$

where c and L are constants $\tilde{y} = y - y_A$. But $q_+ = q$ at A, so q_+ and q_- are $O(q)$ in the cusp region. Hence the cusp region has size l given by

$$\omega l \ln(L/l) \sim q \tag{71}$$

leading to the estimate

$$a \sim |(q/\omega)/\ln(L\omega/q)|^{-1/2}. \tag{72}$$

Table VII shows that this agrees roughly with the results for small q.

TABLE VII. A test of the estimate (72). The third figure in q and in a is questionable.

ω	q	a	$a\lvert q/\ln q\rvert^{1/2}$
6.0	0.225	2.17	0.844
6.025	0.201	2.36	0.834
6.05	0.173	2.71	0.852
6.075	0.138	3.14	0.828

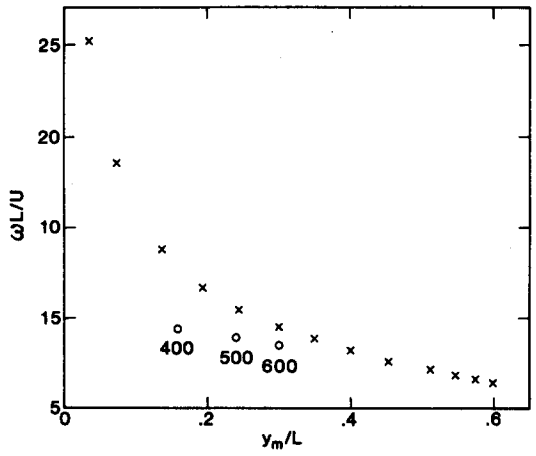

FIG. 11. A comparison of the inviscid value X of $\omega L/U$ as a function of y_m/L with Fornberg's solution of the Navier–Stokes equations ⊙ at Reynolds numbers 400, 500, and 600.

VI. CONCLUSIONS

We have computed two families of Batchelor flows, namely, the Sadovskii vortex and the rotational corner flow. Both families exhibited the maximum possible symmetry. In the range of values of q for which accurate computation proved possible we found no evidence of bifurcations to solutions with less symmetry. However, the singular nature of the limit $q \to 0$ prevents us from drawing a firm conclusion about the existence of nonsymmetric solutions for small q. Moreover, there may be branches of solutions unconnected to the present branch. Also, we have not considered, for example, the possibility of Sadovskii solutions with inward pointing cusps.

We have given order-of-magnitude estimates of the formation of the high curvature region that forms as $q \to 0$, but this limit remains a challenging analytical problem.

Finally, we examine Fornberg's[9] suggestion that the Sadovskii vortex is an approximation to the wake behind a circular cylinder at large Reynolds numbers. Fornberg does not estimate c_2, so we have eliminated it and plotted in Fig. 11—$\omega L/U$ against y_m/L, where U is the mainstream, $2L$ the length, and y_m the amplitude [Fig. 2(a)] of the Sadovskii solution. The comparison is encouraging and it will be interesting to compare with Navier–Stokes solutions at even higher Reynolds numbers, when these are available.

ACKNOWLEDGMENTS

This work was supported by the U.S. Department of Energy, Applied Mathematical Sciences (DE-AS03-76ER72012).

APPENDIX: DETAILS OF CORNER FLOW

The complete velocity $v(z)$ due to a point vortex of unit circulation at $z'(\neq z)$ is

$$v(z) = -(i/2\pi)g(z;z',\bar{z}'), \tag{A1}$$

where

$$g = \frac{1}{z-z'} - \frac{1}{z-\bar{z}'} - \frac{1}{z+\bar{z}'} + \frac{1}{z+z'}. \tag{A2}$$

It is immediate that the contribution to the velocity at $z(\theta)$ on S due to the vortex sheet is [cf. (23)]

$$Q^{(1)}_{\pm}(\theta) = \mp\frac{1}{2}\frac{G(\theta)}{dz/d\theta} - \frac{i}{2\pi} \times \fint_0^{\pi} G(\theta')g(z(\theta);z(\theta'),\bar{z}(\theta'))d\theta'. \tag{A3}$$

Next we consider z to be strictly outside the patch P. Then

$$Q^{(2)}(z) = -\frac{i\omega}{2\pi}\int\int_P g(z;z',\bar{z}')dx'\,dy'. \tag{A4}$$

Define $f(z;z',\bar{z}')$ by

$$\frac{\partial f}{\partial z'} = g. \tag{A5}$$

An integral is

$$f = -\ln(z-z') - \frac{(z'-z)}{z-\bar{z}'} - \frac{(z'-z)}{z+\bar{z}'} + \ln(z+z'), \tag{A6}$$

where the constant of integration is chosen to prevent the second and third terms becoming large near A [Fig. 2(b)] and B, respectively. Thus

$$Q^{(2)}(z) = \frac{\omega}{4\pi}\oint_{\partial P} f(z;z',\bar{z}')d\bar{z}'. \tag{A7}$$

Integration by parts removes the logarithmic terms to yield

$$Q^{(2)}(z) = \frac{\omega}{4\pi}\oint_{\partial P}\left(\frac{\bar{z}-\bar{z}'}{z-z'} - \frac{\bar{z}+\bar{z}'}{z+z'}\right)dz + \frac{\omega}{4\pi}\oint_{\partial P}\left(\frac{z-z'}{z-\bar{z}'} + \frac{z-z'}{z+\bar{z}'}\right)d\bar{z}. \tag{A8}$$

The contributions to $Q^{(2)}$ from the portion of ∂P formed by the axes can be found analytically, so only the contribution from S need be found numerically; the details are straightforward.

The second method can be applied to the corner flow by means of a quadratic map. If (x,y) are the coordinates in the corner plane, with streamfunction $\psi = -\alpha xy$ at ∞, $\hat{x} = x^2 - y^2$, $\hat{y} = 2xy$ maps the corner vortex into a Sadovskii vortex in the $(\hat{x},\hat{y})$ plane in a stream $U = \alpha/2$, except that the interior vorticity is now not constant and Ψ satisfies the equation

$$\nabla^2\Psi = -\omega/4\hat{r}, \quad \hat{r} = (\hat{x}^2 + \hat{y}^2)^{1/2}. \tag{A9}$$

An appropriate solution of this equation, with Ψ constant on $y = 0$ is

$$\Psi = \frac{-\omega\hat{r}}{4} - \frac{\omega}{2\pi}\left[\hat{y}\log\hat{r} + \hat{x}\left(\tan^{-1}\frac{\hat{y}}{\hat{x}} - \frac{\pi}{2}\right)\right] + \frac{\omega\hat{y}}{2\pi}. \tag{A10}$$

The last term is included to ensure that $\partial\Psi/\partial\hat{y} = 0$ at $\hat{x} = \pm 1, \hat{y} = 0$; otherwise $d\phi/d\theta$ does not vanish at the end points and the representation (56) converges very slowly.

Extra terms can be added to make $\partial^2\Psi/\partial\hat{y}\,\partial\hat{x}$ vanish at the cusps, but this was not done.

If the dimensions of the sides of the vortex are 1 and h, the appropriate representation of the shape of S is again (20) and (21). The calculation proceeds as before with differences in detail as a result of the fact that the velocities have to be transformed back into the corner plane before applying the boundary condition on the pressure. There is one difference in principle. There is now no D'Alembert paradox, so Eqs. (58) are now independent. However, h is now a further unknown so the counting for the full nonsymmetrical problem is correct. If one assumes symmetry, then $h = 1$ and an equation is also lost, so the counting is still correct.

[1]G. K. Batchelor, J. Fluid Mech. **1**, 388 (1956).
[2]S. Childress, Phys. Fluids **9**, 860 (1966).
[3]V. S. Sadovskii, Appl. Math. Mech. **35**, 773 (1971).
[4]R. T. Pierrehumbert, J. Fluid Mech. **99**, 129 (1980).
[5]P. G. Saffman and S. Tanveer, Phys. Fluids **25**, 1929 (1982).
[6]F. T. Smith, J. Fluid Mech. **155**, 175 (1985).
[7]F. T. Smith, J. Eng. Math. **20**, 271 (1986).
[8]S. I. Chernyshenko, Royal Aircraft Establishment library translations Report No. 2133, 1983.
[9]B. Fornberg, J. Comput. Phys. **61**, 297 (1985).
[10]J. H. B. Smith, in *Vortex Motion* (Vieweg, Braunschweig, 1982), p. 157.
[11]D. I. Pullin, J. Fluid Mech. **108**, 401 (1981).
[12]B. Maskew, J. Aircraft **14**, 188 (1977).
[13]M. Tanaka, J. W. Dold, M. Lewy, and D. H. Peregrine, J. Fluid Mech. **185**, 235 (1987).
[14]B. Chen and P. G. Saffman, Stud. Appl. Math. **62**, 1 (1980).